

Tunable edge states and their robustness towards disorder

M. Malki* and G. S. Uhrig

Lehrstuhl für Theoretische Physik 1, TU Dortmund, Germany

(Dated: March 10, 2022)

The interest in the properties of edge states in Chern insulators and in \mathbb{Z}_2 topological insulators has increased rapidly in recent years. We present calculations on how to influence the transport properties of chiral and helical edge states by modifying the edges in the Haldane and in the Kane-Mele model. The Fermi velocity of the chiral edge states becomes direction dependent as does the spin-dependent Fermi velocity of the helical edge states. Additionally, we explicitly investigate the robustness of edge states against local disorder. The edge states can be reconstructed in the Brillouin zone in the presence of disorder. The influence of the width and of the length of the system is studied as well as the dependence of the edge states on the strength of the disorder.

PACS numbers: 03.65.Vf, 61.43.Bn, 72.80.Ng, 71.23.-k

I. INTRODUCTION

A. General context

Since the discovery of the integer and the fractional quantum Hall effect^{1,2} topological phenomena have become an important field of research in condensed matter physics. The edge states³ occurring in the quantum Hall effect are localized exponentially at the boundaries of the sample. They are protected by the topological properties of the band structure in the bulk. As shown by Thouless et al.⁴ the number of edge states corresponds to the Chern number ν of the filled electronic bands and implies the famous quantized Hall conductivity $\sigma_{xy} = \nu e^2/h$. The description of the quantum Hall effect by topological invariants⁵⁻⁸ is based on the Berry phase⁹.

In order to mimic the integer quantum Hall effect in a lattice model *without* external magnetic field Haldane has proposed the first Chern insulator¹⁰. In addition to nearest-neighbor hopping on a honeycomb lattice, the proposed Haldane model comprises a staggered magnetic flux which induces complex next-nearest-neighbor hopping elements while the translational symmetry is preserved. Averaged over a unit cell of the lattice the magnetic flux vanishes. However, for certain values of the phases a finite magnetic field cannot be distinguished from a vanishing average magnetic field because phases of multiples of 2π cannot be distinguished from vanishing phases¹¹.

In order to realize a Chern insulator the time reversal symmetry (TRS) must be broken. Nontrivial Chern numbers imply chiral edge states also in the absence of an external magnetic field extending the concept of the usual quantum Hall effect. In the context of topologically protected edge states the term ‘chiral’ means that the electrons only propagate in one direction along one edge. If no magnetic field is involved this effect is called the *anomalous* quantum Hall effect¹²⁻¹⁴.

The Kane-Mele model¹⁵⁻¹⁷ represents a crucial extension of the Haldane model including the spin degree of freedom. This renders the preservation of the TRS possible because one spin species realizes the time-reversed

replica of the other. The Kane-Mele model was suggested to describe the effect of spin-orbit interaction on the electronic band structure of graphene in the low-energy regime, but it turned out that the spin-orbit interaction in graphene is too weak to produce noticeable effects. Nevertheless, the Kane-Mele model provides fascinating theoretical insights.

Due to the preservation of the TRS in the Kane-Mele model it cannot display a net charge current at the edges. Instead, a net spin current is possible. This phenomenon is referred to as the quantum spin Hall effect (QSHE) which can be attributed to the topological \mathbb{Z}_2 invariant^{16,18,19} implying helical edge states²⁰. These topologically protected edge states are called ‘helical’ because they have a spin filtering property, i.e., the spins \uparrow propagate in one direction while the spins \downarrow propagate in the opposite direction along the same edge. As a result, the QSHE implies a quantization of the spin Hall conductivity. Basically, materials displaying the QSHE and characterized by the \mathbb{Z}_2 topological invariant are referred to as \mathbb{Z}_2 topological insulators^{17,21}.

Since the QSHE is too weak in graphene to be measurable, Bernevig, Hughes, and Zhang proposed a model²² for the QSH phase in HgTe quantum wells where the spin-orbit coupling is much stronger. Soon after the theoretical proposal the QSH phase has been observed experimentally in a 2D HgTe/CdTe quantum well^{23,24}. Another experimental observation of the QSHE was realized in InAs/GaSb quantum wells^{25,26}. The discovered QSHE is only measured at low temperatures up to 40 K. Theoretical calculations²⁷ predict a possible realization of the QSHE in germanium with a large energy gap corresponding to 277 K. The calculated energy gap of the low-buckled honeycomb structure of germanium results from the stronger spin-orbit coupling so that this system is a candidate for detecting the QSHE at higher temperatures.

Historically, the QSHE was measured first in 2D topological insulators. A Chern insulator was considered unlikely to be realized. But very recently, progress has been achieved towards 2D Chern insulators. The first observation of the anomalous quantum Hall effect was made

in thin ferromagnetic Chern insulators^{28–30}. It could be observed up to temperatures of a few Kelvin. Theoretical proposals indicate that Chern insulators near room temperature are possible in thin ferromagnetic Chern insulators³¹ or in superlattices of gold atoms on single-vacancy graphene^{32,33}.

An alternative realization has been achieved using ultracold fermionic ⁴⁰K atoms in a periodically modulated optical lattice³⁴. This method could implement the Haldane model in an experimental setup. A particular asset of this route is the tunability of the physical properties.

B. Present objectives

Due to their topological protection, edge states may carry currents without dissipation and they are protected against disorder to some extent, see below. This robustness makes them attractive to applications. With this long-term goal in mind, we set out to study the influence of controllable external parameters on the transport behavior of topological edge state as well as to study the effect of noncontrollable features such as disorder. We do not focus on the DC conductivity as has been done before, see for instance Refs. ^{35,36}. We choose the Fermi velocity v_F as the measurable quantity of interest in order to gain understanding which is complementary to the existing literature.

The Fermi velocity is a key quantity in transport behavior representing the group velocity of a transmitted charge or spin signal. Thus, we aim at tuning the Fermi velocity which quantifies how fast a signal is transmitted. A previous observation in the Kagome lattice¹¹ revealed that the Fermi velocity depends on the chosen shape of the edge. Further investigations in the Haldane model³⁷ showed that by decorating one edge of the honeycomb lattice the Fermi velocity can be influenced strongly. We extend this observation by considering decorating both edges.

Next, we transfer the idea of decoration to the Kane-Mele model, i.e., to helical edge states. An explicit Rashba coupling³⁸ and its effect on the Fermi velocity is also studied. The decoration of the edges of the Kane-Mele model leads to a tunable spin-dependent Fermi velocity which suggests the applicability of tunable transmission speeds in spintronics^{39,40}.

Finally, we study the influence of local disorder on the edge states. Since edge modes are due to nontrivial topological invariants it is assumed that they are protected against disorder. However, various experiments show that the signatures of topological phases are much more prominent in high-purity samples¹⁷ than in samples of lower quality. Thus, we intend to investigate the influence of disorder by explicit calculations. For simplicity, we study the robustness of the chiral edge states in the Haldane model on the honeycomb lattice.

Local disorder breaks the translational invariance. By calculating the modulus squared of the overlap of the

eigenwave functions of the disordered system with the eigenedge modes in the clean system we define a transition probability. The maximization of this quantity is used to reconstruct the momenta of the edge states. The dependence of the transition probability on the width, the length of the system as well as on the strength of the local disorder is examined. We find that the disorder may not exceed certain thresholds in order to preserve the characteristic transport properties of the edge modes.

II. DECORATION OF THE HALDANE MODEL

For the sake of completeness, we recap results for decorated edges in the model without spin³⁷. The results are important for the comparison with the results in the modified and extended models with spin. Moreover, they serve as reference for the disordered Haldane model which we investigate in Sec. IV.

The complete Hamiltonian of the model can be divided into two contributions

$$\mathcal{H} = \mathcal{H}_{\text{strip}} + \mathcal{H}_{\text{decor}} \quad (1a)$$

with

$$\mathcal{H}_{\text{strip}} = t \sum_{\langle i,j \rangle} c_i^\dagger c_j + t_2 \sum_{\langle\langle i,j \rangle\rangle} e^{i\nu_{ij}\phi} c_i^\dagger c_j \quad (1b)$$

$$\mathcal{H}_{\text{decor}} = \sum_{i\gamma} \left[\lambda_\gamma \left(c_{d(i)}^\dagger c_i + c_i^\dagger c_{d(i)} \right) + \delta_\gamma c_{d(i)}^\dagger c_{d(i)} \right]. \quad (1c)$$

The corresponding honeycomb lattice with decorated edges is shown in Fig. 1. The Hamiltonian $\mathcal{H}_{\text{strip}}$ comprises a real hopping element between nearest neighbor (NN) sites and a complex hopping element between next-nearest neighbor (NNN) sites. The symbol $\langle i, j \rangle$ denotes a pair of NN sites while $\langle\langle i, j \rangle\rangle$ denotes a pair of NNN sites. The hopping parameter t is real and serves as energy unit henceforth. The lattice constant a is set to unity. The complex hopping element is given by the combination of the positive real parameter t_2 and a phase ϕ . The inclusion of the nonvanishing phase breaks the TRS as is necessary for obtaining nontrivial Chern numbers.

The sign of the phase is determined by

$$\nu_{ij} = \text{sgn}(\hat{d}_1(ij) \times \hat{d}_2(ij))_z = \pm 1 \quad (2)$$

where one reaches site j from site i by a NN hop to site i' and a second NN hop from i' to j . Then, $\hat{d}_1(ij)$ stands for the unit vector from i to i' and $\hat{d}_2(ij)$ for the unit vector from i' to j . The complex hopping elements with phase ϕ are shown in blue (dark gray) while the hopping elements with phase $-\phi$ are shown in red (light gray) in Fig. 1.

The Hamilton operator of the decorating sites $\mathcal{H}_{\text{decor}}$ consists of two parts. One part describes the additional sites at the top whereas the other part describes the bottom sites ($\gamma \in \{t, b\}$). If the outermost sites of the undecorated honeycomb lattice are denoted by j the adjacent

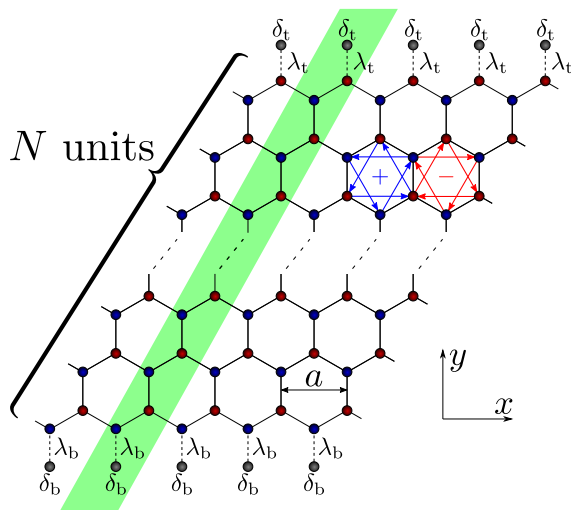


FIG. 1: (Color online) Sketch of a strip in the honeycomb lattice with NN hopping (black bonds). The green (light shaded) area displays a unit cell in the x direction which consists of $2N + 2$ sites including the decorating sites. The honeycomb with blue arrows illustrates the complex hopping elements to NNN sites with phase ϕ while the honeycomb with red arrows illustrates the hopping elements with phase $-\phi$, see Eq. (2). The top and the bottom edge are decorated by additional sites which are coupled weakly ($\lambda_\gamma < t$) to the bulk sites. These decorating sites are subject to a local potential δ_γ . The index γ takes the value t (top) or b (bottom). The lattice constant a is set to unity.

decorating sites are labeled $d(j)$. The hopping elements between the outermost sites and the attached decorating sites are modified by the factor λ_γ . Generically, we consider an attenuation so that $0 \leq \lambda_\gamma \leq t$ holds. The on-site energy of the decorating sites are denoted by δ_γ . It can be thought to be generated by a gate voltage which changes the electric potential of the decorating sites³⁷.

The phase diagram of the Haldane model on a bulk honeycomb lattice without boundaries can be found for instance in Refs. 10,19. Calculating the dispersion on a finite strip, see Fig. 1, of the system provides the chiral edge states. Coupling the decorating sites to the honeycomb strip does not alter the topological characteristics of the system. The phase ϕ is set to $\pi/2$ in order to maximize the gap. To create rather flat energy bands we set $t_2 = 0.2t$ as in Ref. 37. The Fermi level is set to $\varepsilon_F = 0$.

To illustrate the impact of the modification we calculate the dispersion of both edge modes and compare it to the dispersion in the undecorated Haldane model. In the following, we investigate a strip of finite height in the y direction whereas the strip is infinitely extended in the x direction, see Fig. 1. Due to the translational symmetry in the x direction, the wave number k_x represents a good quantum number. At fixed k_x , one obtains a $(2N+2) \times (2N+2)$ one-particle matrix which can be diagonalized numerically. The dispersive modes within the gap of the bulk Haldane model are the edge modes. Due to their exponential localization at the edges their dis-

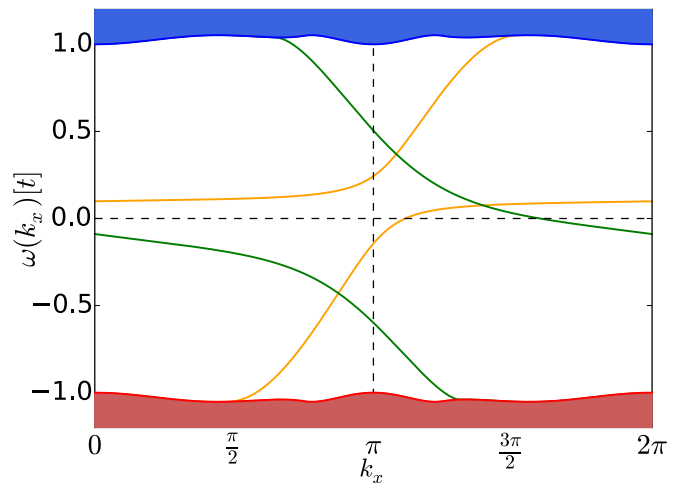


FIG. 2: (Color online) (a) Dispersion of the edge states with $t_2 = 0.2t$, $\phi = \pi/2$, $\lambda_t = 0.2t$, $\delta_t = 0.1t$, $\lambda_b = 0.6t$, and $\delta_b = -0.1t$. The right-moving edge state marked in orange (light gray) is located at the top edge while the left-moving edge state marked in green (dark gray) is located at the the bottom edge. The filled areas indicate the continua of the bulk states. The Fermi velocity $v_F = \partial\omega/\partial k_x|_{\varepsilon_F}$ of both edges modes are independent of each other.

persion converges quickly upon increasing the number N of units in the strip. The calculations in this work are based on strips with $N = 60$ units which turns out to be sufficiently wide.

An example of a dispersion with different parameters for both edges is shown in Fig. 2. The filled areas represent the continua stemming from the modes for all possible values of k_y . Our main focus lies on the investigation of the edge modes of which the energies are between the lower band edge of the upper continuum (blue, darker shading) and the upper band edge of the lower continuum (red, lighter shading).

Upon coupling the decorating sites to the honeycomb strip, i.e., $\lambda_\gamma \neq 0$, the dispersions of the edge modes display an ‘avoided crossing’ (or ‘level repulsion’) due to the hybridization with the local modes from the decorating sites. In the case of small values of λ , see right mover in Fig. 2, the edge states have a rather flat band. Increasing λ leads to a stronger repulsion between the edge modes near the zone boundary $k_x = \pi$ so that the dispersion acquires stronger momentum dependence, see left mover in Fig. 2.

Besides the coupling λ_γ , the decorating sites can be influenced by the local potentials δ_γ . Increasing the local energy of the decorating sites counteracts the hybridization because the tendency of an electron to visit the decorating sites is decreased if these sites differ in energy from the bulk sites. In this way, the decorating sites can be smoothly switched off. Then, the Fermi velocity converges to the Fermi velocity v_{F0} without decoration.

The dependence of the Fermi velocity on the parameters of the decorated model has been studied quanti-

tatively for a single decorated edge³⁷. To prove the independence of the chiral edge modes explicitly we calculated the Fermi velocity of both edges while tuning parameters of only one edge. The Fermi velocity of the unaltered edge remains unaffected to the tenth digit. We stress that the relative coupling λ_γ and the local potential δ_γ provide controllable parameters to tune the Fermi velocity of the edge mode independent from the other edge mode. Furthermore, different decorations at the top and at the bottom edge enable us to realize different Fermi velocities $v_{F,\gamma}$ so that the velocities become direction-sensitive.

III. DECORATION OF THE KANE-MELE MODEL

Here, we investigate the impact of decorated edges on the helical edge states of the Kane-Mele model which includes the spin degree of freedom in such a fashion that it preserves the TRS. The Hamiltonian reads

$$\mathcal{H} = \mathcal{H}_{\text{strip}} + \mathcal{H}_{\text{decor}} \quad (3a)$$

with

$$\begin{aligned} \mathcal{H}_{\text{strip}} = & t \sum_{\langle i,j \rangle \alpha} c_{i\alpha}^\dagger c_{j\alpha} + it_2 \sum_{\langle\langle i,j \rangle\rangle \alpha\beta} \nu_{ij} c_{i\alpha}^\dagger \sigma_{\alpha\beta}^z c_{j\beta} \\ & + it_\tau \sum_{\langle i,j \rangle \alpha\beta} c_{i\alpha}^\dagger (\sigma_{\alpha\beta} \times \hat{d}_{ij})_z c_{j\beta} \end{aligned} \quad (3b)$$

and

$$\begin{aligned} \mathcal{H}_{\text{decor}} = & \sum_{i\gamma\alpha} \left[\lambda_\gamma \left(c_{d(i)\alpha}^\dagger c_{i\alpha} + c_{i\alpha}^\dagger c_{d(i)\alpha} \right) \right. \\ & \left. + \delta_\gamma c_{d(i)\alpha}^\dagger c_{d(i)\alpha} \right] \end{aligned} \quad (3c)$$

on the honeycomb lattice similar to the decorated Haldane model from the previous section, see Fig. 1. In the Kane-Mele model, each site can host two electrons with spin quantum number denoted by $\alpha, \beta \in \{\uparrow, \downarrow\}$. The Hamilton operator of the strip contains three contributions. The first term describes the usual tight-binding hopping t between NN sites. As before the hopping parameter t is real and used as the energy unit.

Kane and Mele¹⁵ argued that the second hopping term $\propto t_2$ is induced by spin-orbit interaction. The hopping parameter t_2 is real and the sign depends on the NNN sites i and j as given by ν_{ij} defined in (2). The NNN term is closely related to the NNN hopping in the Haldane model. Considering each spin species separately, the corresponding Hamiltonian with NN and NNN hopping violates the TRS. It equals the Haldane Hamiltonian at $\phi = \pm\pi/2$ for either $S^z = +1/2$ or $S^z = -1/2$. The Kane-Mele model comprises two decoupled Haldane models with opposite phases. Since the time reversal transformation $T = \exp(-i\pi S^y)K$ maps one onto the other their combination preserves the TRS¹⁹.

The last term in $\mathcal{H}_{\text{strip}}$ proportional to t_τ describes a Rashba term^{15,38} which can also result from spin-orbit coupling in the presence of a perpendicular electric field or a certain interaction with a substrate. The hopping element parameter t_τ of the Rashba term is real. The Rashba term violates the conservation of the total S^z component so that the two Haldane models for $S^z = \pm 1/2$ are coupled for $t_\tau \neq 0$.

The Hamiltonian of the decorating sites at the edge is chosen to be spin independent for simplicity, similar to the decoration of the Haldane model. So the notation will be the same except that an additional index is used to denote the spin.

The topological phases of the Kane-Mele model are classified by a \mathbb{Z}_2 invariant. The phase diagram of the bulk Kane-Mele model including the Rashba coupling is known^{16,19}. We detect the presence of helical edge states by calculating the dispersion on a strip of finite width as before.

First, we set the Rashba coupling to zero so that our results can be directly linked to the results for the decorated Haldane model. For $\lambda_\gamma = \delta_\gamma = 0$, the original Kane-Mele model on a strip is retrieved. The corresponding Hamiltonian consists of two decoupled Haldane Hamiltonian each of which displays its own chiral edge states. The chiral edge states of the spin \uparrow part move in opposite direction to the chiral edge states of the spin \downarrow part because the phase of their NNN hopping element is opposite. The two chiral edge states with opposite spins constitute a pair of counterpropagating edge modes at each edge. As shown in the previous section, the top edge can be modified independently of the bottom edge. This also holds true for the Kane-Mele model. Therefore, we only consider the decoration of the top edge in the following for brevity.

In the Kane-Mele model, the Fermi velocities of the edge modes are spin-dependent. Except for this difference, one can carry over the basic considerations that we developed for the decorated Haldane model. Figure 3 illustrates this point. The helical edge states of the bottom edge are the same edge states as in an undecorated Kane-Mele strip because the bottom edge is undecorated. The dispersion of the modes at the top edge display the effect of the ‘avoided crossing’ combined with a certain shift of the dispersion due to the local potential. This is in line with the results for the Haldane model.

Due to TRS, the dispersions display two mirror planes at the momenta invariant under time reversal: $k_x = 0$ or $k_x = \pi$. This property is based on Kramer’s theorem⁴¹. Kramer’s theorem predicts crossing points of the counterpropagating edge states at the time reversal invariant momenta. The two crossing modes represent the famous Kramer’s pairs. Their degeneracy is robust against time reversal symmetric perturbations. The level repulsion of the ‘avoided crossing’ leads to a Kramer doublet located at $k_x = 0$. The number of Kramer’s doublets at one edge must be odd in the topologically nontrivial phase because it is related to the \mathbb{Z}_2 topological invariant¹⁷.

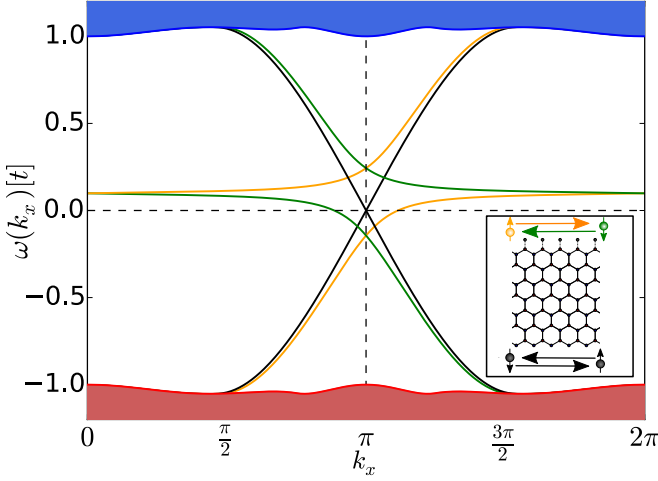


FIG. 3: (Color online) Dispersion of the edge states with $t_2 = 0.2t$, $\lambda_t = 0.2t$ and $\delta_t = 0.1t$. The filled areas indicate the continua of the bulk states. The edge states located at the top edge are shown in color (gray). The spin \uparrow mode propagating to the right is marked in orange (light gray) while the spin \downarrow mode counterpropagating to the left is marked in green (dark gray). The dispersion of the edge states at the lower boundary are displayed in black. The schematic sketch in the inset clarifies the assignments.

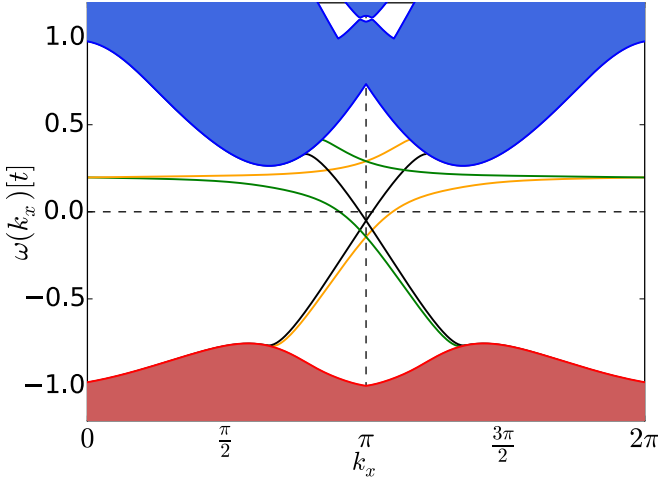


FIG. 4: (Color online) Dispersion of the edge states at finite Rashba coupling at $t_2 = 0.2t$, $t_r = 0.8t$, $\lambda_t = 0.2t$ and $\delta_t = 0.2t$. The filled areas indicate the continua of the bulk states. The edge states located at the top edge are shown in color (gray). The spin \uparrow mode propagating to the right is marked in orange (light gray) while the spin \downarrow mode counterpropagating to the left is marked in green (dark gray). The dispersions of the edge states at the lower boundary are displayed in black.

The inclusion of a finite Rashba coupling $t_r \neq 0$ violates the S^z conservation and the two Haldane models hybridize. The Rashba coupling alone without the imaginary NNN hopping does not lead to a topologically nontrivial phase¹⁹ which means that the imaginary NNN hopping is indispensable for the anomalous QSHE in the

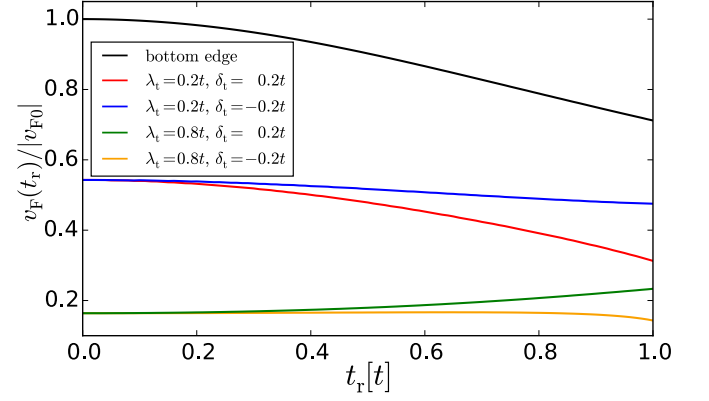


FIG. 5: (Color online) Fermi velocity $v_F = \partial\omega/\partial k_x|_{\varepsilon_F}$ of the right-moving edge modes relative to the original v_{F0} without decorated edges vs. the Rashba coupling t_r at $t_2 = 0.2t$ for various decorations of the top edges and undecorated bottom edges.

Kane-Mele model. But the Rashba coupling reduces or enhances the bulk gap and influences the edge states in this way. An exemplary dispersion of the helical edge states in the Kane-Mele model is depicted in Fig. 4 where the Rashba coupling t_r has been chosen fairly large in order to show its influence on the bulk and on the edge states. For not too large values of the Rashba coupling the qualitative features of the bulk and of the helical edge states remain unaltered.

The counterpropagating edge modes forming a Kramer's pair still cross each other as long as the TRS is preserved and the bulk gap does not close. If the gap is reduced by tuning t_r the bulk states repel the edge modes. The effect can be seen in Fig. 4 where the energies of the Kramer's pair at the bottom edge are shifted downwards. As a result, v_F can increase or decrease upon switching on the Rashba coupling as shown in Fig. 5. Since the particle-hole symmetry is broken by the Rashba coupling the inclusion of the local potentials at the decorating sites is no longer symmetric so that the effect of a negative potential differs from the one of a positive potential. Even the sign of the effect can change.

In a system preserving TRS the addition of a finite amount of unpolarized charge at one edge does not lead to a net charge current because the two counterpropagating modes compensate in charge due to their equal Fermi velocities. In order to create a net charge current the TRS must be broken. One possible way is to include a spin-dependent decoration. This can be accomplished for example by proximity-induced ferromagnetic exchange at the interface with a magnetic insulator⁴². To demonstrate this basic idea we replace $\mathcal{H}_{\text{decor}}$ by

$$\mathcal{H}_{\text{decor}} = \sum_{i,\gamma,\alpha} \left[\lambda_\gamma \left(c_{d(i)\alpha}^\dagger c_{i\alpha} + c_{i\alpha}^\dagger c_{d(i)\alpha} \right) + \delta_\gamma c_{d(i)\alpha}^\dagger \sigma_{\alpha\alpha}^z c_{d(i)\alpha} \right]. \quad (4)$$

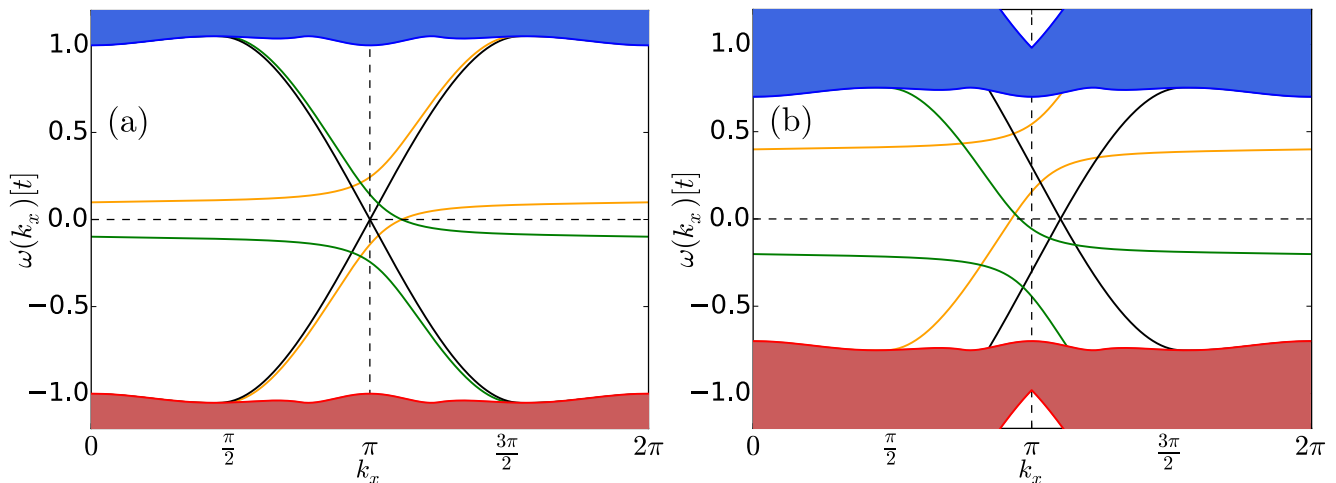


FIG. 6: (Color online) (a) Dispersion of the edge states at $t_2 = 0.2t, t_r = 0, \lambda_t = 0.2t$, and $\delta_t = 0.1t$. The filled areas indicate the continua of the bulk states. The edge states located at the top edge are shown in color (gray). The spin \uparrow mode propagating to the right is marked in orange (light gray) while the spin \downarrow mode counterpropagating to the left is marked in green (dark gray). The dispersion of the edge states at the lower boundary are displayed in black. (b) Dispersion of the edge states at $t_2 = 0.2t, t_r = 0, h_z = 0.3t$ in Eq. (5), $\lambda_t = 0.2t$, and $\delta_t = 0.1t$.

The change relative to Eq. (3c) is that the local potential depends on the Pauli matrix σ_z . To illustrate the difference to the previous decoration we depict the resulting dispersion in Fig. 6(a) keeping all other parameters as before. Due to the spin-dependent decoration of the top edge the corresponding Kramer's doublets do no longer exist. Furthermore, the counterpropagating edge modes do not cancel each other. Hence, a net charge and spin current is possible.

Another possible way to break the TRS is to split the two spin states by adding a ferromagnetic exchange field

$$\mathcal{H}_{\text{FMX}} = h_z \sum_{i,\alpha} (c_{i\alpha}^\dagger \sigma_{\alpha\alpha}^z c_{i\alpha} + c_{d(i)\alpha}^\dagger \sigma_{\alpha\alpha}^z c_{d(i)\alpha}) \quad (5)$$

to the decorated model in Eq. (3a). In contrast to the previous example, the exchange field is present at all sites. This may be realized by magnetic doping^{43–45}. For vanishing Rashba coupling $t_r = 0$, the influence of the exchange field can be easily understood by regarding the Kane-Mele model as two decoupled decorated Haldane models of which the chemical potentials are shifted in the opposite directions. Kramer's doublets do no longer exist, see Fig. 6(b).

IV. ROBUSTNESS OF THE EDGE STATES AGAINST POTENTIAL DISORDER

So far, we analyzed how an important transport property of the edge states, the Fermi velocity, can be controlled by tuning parameters. But there are also uncontrollable properties of a solid state system. For instance, imperfections of all kinds such as impurities, defects or vacancies in the lattice structure can never be fully excluded. We cannot consider them exhaustively here. But

we aim at a first study of the robustness of the edge states with respect to disorder. To this end, we consider disorder in the local potentials.

The edge states emerge as a result of the discontinuity of topological invariants at the edges of a system. Since a topological invariant is a global property of the bulk system it is expected that the edge states are protected as long as the disorder does not change the global properties of the bulk system. We want to study this explicitly. To this end, we investigate the Haldane model (1b) on a finite strip of the honeycomb lattice as shown in Fig. 7. We consider a strip of N_x columns of a finite width of N_y units so that there are $2N_x N_y$ sites. We add a random local potential at each site to the Haldane model (1b) to simulate the disorder. The random energies are taken from a continuous uniform distribution in the interval $[-\sqrt{3}\sigma, \sqrt{3}\sigma]$ where the standard deviation is given by σ . This is the control parameter for the strength of the local disorder. We also investigated random local potentials which are Gaussian distributed, but the results do not differ fundamentally.

The translation symmetry in the x direction is no longer preserved due to disorder. In order to establish a link to the system without disorder we continue to consider periodic boundary conditions. By diagonalizing the $(2N_y N_x) \times (2N_y N_x)$ matrix encoding hopping and local energies we obtain the eigenenergies. The corresponding eigenvectors cannot be classified directly according to their momenta k_x . The eigenstates are given in spatial representation by

$$|\psi\rangle = \sum_{x,y} c(x,y) |x,y\rangle, \quad (6)$$

where x and y correspond to the discrete coordinates of the lattice sites. In order to map the eigenstates of the

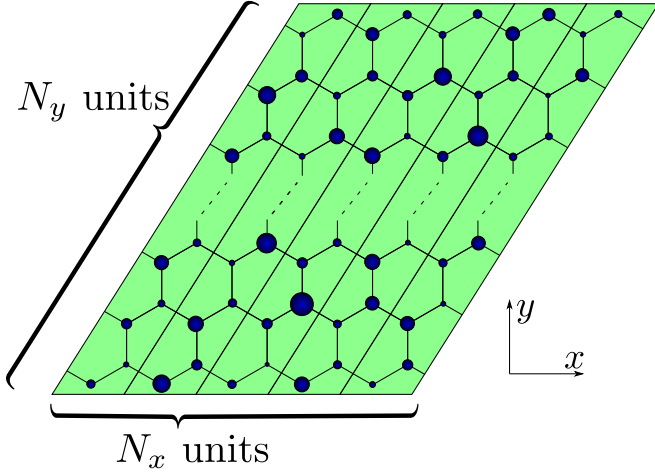


FIG. 7: (Color online) Sketch of a finite strip of honeycomb lattice consisting of N_x columns of finite width of N_y units. Each column is enclosed by thin black lines. The different sizes of the dots illustrate the random local potentials of a disorder configuration.

disordered system to the eigenstates of the clean system we express the edge states, right- and left-moving ones, of the clean system in real space. Denoting the wave function of an edge state by $|\psi_{cl}\rangle(k_x)$ it reads

$$\begin{aligned} |\psi_{cl}\rangle(k_x) &= \sum_y d(k_x, y) |k_x, y\rangle \\ &= \sum_{x,y} d(k_x, y) \frac{e^{-ik_x x}}{\sqrt{N}} |x, y\rangle. \end{aligned} \quad (7a)$$

In comparison to the representation (6) we deduce

$$c_{k_x}(x, y) = d(k_x, y) \frac{e^{-ik_x x}}{\sqrt{N}}. \quad (7b)$$

The possible momenta are given by $k_x = 2\pi n_x/N_x$ with $n_x = \{0, 1, \dots, N_x - 1\}$.

In order to assign a momentum k_x to an energy of an edge state of the disordered system we search for the largest overlap with a clean edge mode, i.e., we maximize $|\langle\psi|\psi_{cl}\rangle|^2(k_x)$ by varying k_x . The momentum k_x which maximizes this overlap is the one assigned to the eigenstate of the disordered system. The overlap can be interpreted as transition probability and is calculated by

$$|\langle\psi|\psi_{cl}\rangle|^2(k_x) = \left| \sum_{x,y} c^*(x, y) c_{k_x}(x, y) \right|^2. \quad (8)$$

Following this procedure, we reconstruct the dispersion of the edge state in the Brillouin zone as shown in Fig. 8 for $\sigma = 0.1t$. Typically, we consider a system of $N_y = 50$ and $N_x = 21$ leading to $2N_y N_x = 2100$ eigenenergies from which we select the energies corresponding to the edge state by maximizing the transition probability (8). The dispersions of the edge modes of the clean system

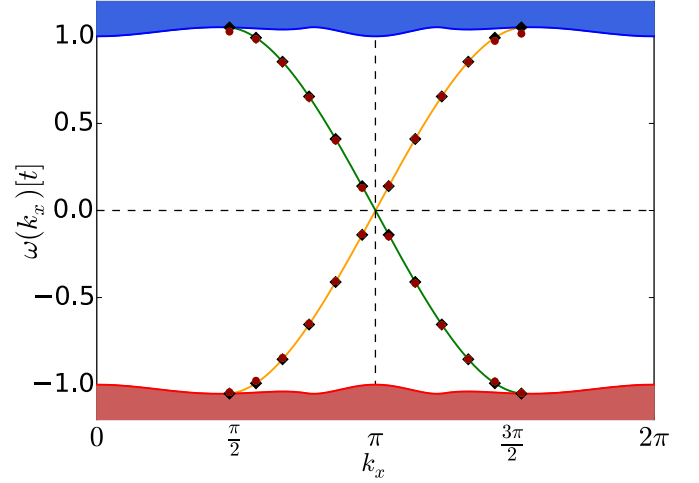


FIG. 8: (Color online) Dispersion of the edge states with $t_2 = 0.2t$ and $\phi = \pi/2$ of the Haldane model. The filled areas indicate the continua of the bulk states. The right-moving edge state marked in orange (light gray) is located at the top edge while the left-moving edge state marked in green (dark gray) is located at the bottom edge. The symbols indicate the energies of eigenstates of which the momenta are determined from maximizing the transition probability in (8). The black diamonds are calculated for a clean system with $N_y = 50$ and $N_x = 21$ while the red (gray) circles result from a disordered system with $\sigma = 0.1t$.

computed from the infinite strip ($N_x = \infty$) are shown as solid lines for the sake of comparison. To test the maximization of the transition probability we assign momenta to eigenstates computed for a finite clean system. The results are depicted by black diamonds in Fig. 8 and match the continuous lines perfectly. The red (gray) circles display the eigenenergies at the assigned momenta in a disordered system with $\sigma = 0.1t$. They are still located close to the solid lines, but do not match them perfectly due to the disorder.

We conclude that the qualitative features of the edge states are indeed robust against disorder. The gaplessness of the edge modes is preserved as was to be expected from the topological protection. But also the quantitative aspects are not drastically altered by disorder, at least as long as the disorder strength is not too large.

An important point to study is the influence of the disorder on the bulk gap. If the bulk gap becomes small or even vanishes the topological properties disappear. Increasing disorder reduces the bulk gap. An estimate for this reduction can be derived by assuming that the disorder strength σ behaves similar to an on-site inversion-symmetry breaking term $\varepsilon_i M c_i^\dagger c_i$. Here ε_i takes the values ± 1 depending on whether site i belongs to one sublattice or to the other. The energy gap Δ of the bulk system decreases upon increasing M . Similarly, Δ decreases upon increasing σ as we illustrate in Fig. 9 where the lower band edge $\omega_{unoc} = \Delta/2$ of the unoccupied states and the upper band edge $\omega_{occu} = -\Delta/2$

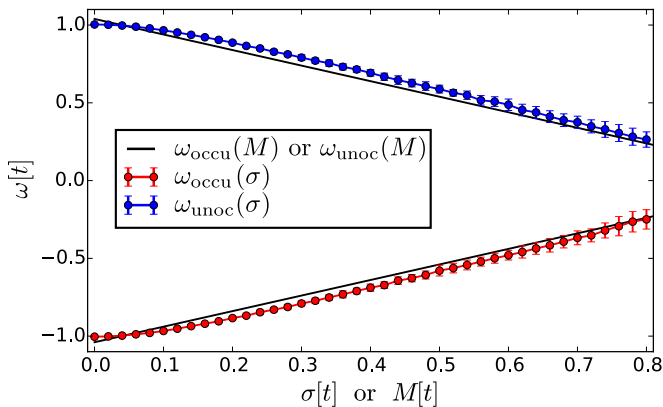


FIG. 9: (Color online) The lower band edge of the conduction band (blue, dark gray) and the maximum energy of the valence band (red, light gray) vs. the disorder strength σ in a system with $N_y = 50$ and $N_x = 21$. The energies are averaged over 60 randomly chosen configurations. The error bars represent a standard deviation. The black lines show the band edges in a clean system as a function of a local inversion-symmetry breaking term $\propto M$, see main text.

of the occupied states are shown. The black solid lines depict the bulk gap as a function of M according to $\Delta = 2|M \pm 3\sqrt{3}t_2 \sin \phi|$ ^{10,45,46}. The symbols show the bulk gap in the disordered sample determined in the following way. For the lower band edge we compute the minimum energy of the eigenstates which *cannot* be assigned to an edge mode of the clean system. Similarly, the upper band edge is determined from the maximum energy of the eigenstates which *cannot* be assigned to an edge mode of the clean system. Of course, this way of determining the bulk gap in the disordered system is a heuristic one and not mathematically rigorous. But the comparison to $\omega_{\text{occu}}(M)$ and $\omega_{\text{unoc}}(M)$ shows good agreement so that we conclude that the estimate works very well.

The energy gap disappears at $M = 3\sqrt{3}t_2 \sin \phi$ ^{10,45,46}. Thus, the estimate predicts that the topological properties will definitely cease to exist for a disorder strength

$$\sigma \approx 3\sqrt{3}t_2 \sin \phi. \quad (9)$$

We stress that the decreasing bulk gap reduces the energy interval in which the edge mode can be identified. Concomitantly, the interval in momentum k_x in which the edge mode can be identified is reduced as well.

Next, we study how well the edge mode can be identified close to the bulk continua. Figure 10 displays the transition probability $|\langle \psi | \psi_{\text{cl}} \rangle|^2(k_x)$ of the edge states in the Brillouin zone. The vertical dashed lines indicate the thresholds where the edge modes enter the bulk continua, i.e., where the energies of the edge modes exceed the estimated bulk gap. It is obvious that around $k_x = \pi$ the transition probability between the edge mode in the disordered system and in the clean system is large. Thus, in particular for low disorder, the identification of the edge mode works reliably. For increasing disorder, the overlap

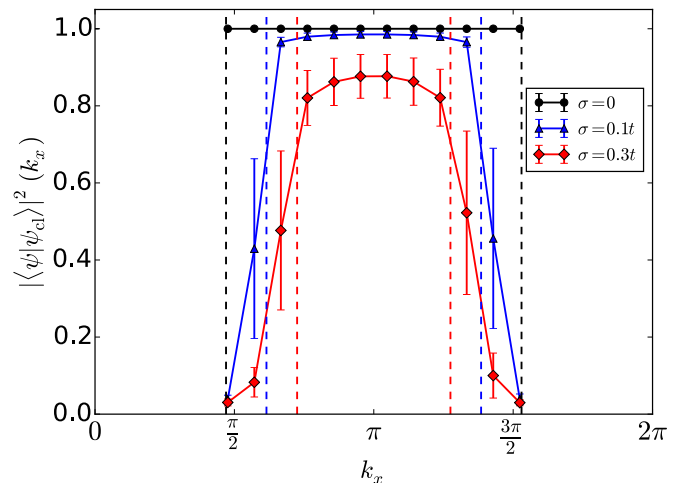


FIG. 10: Transition probability $|\langle \psi | \psi_{\text{cl}} \rangle|^2(k_x)$ of the right-moving edge state averaged over 50 random configurations in a system with $N_y = 50$ and $N_x = 21$ as a function of the momentum k_x . The error bars indicate the standard deviation. The dashed lines indicate at which momenta the energy of the edge mode enters the bulk continua.

decreases gradually. Approaching the band edges at fixed disorder strength, i.e., approaching the dashed line, the overlap decreases rapidly and a clear identification of the edge modes becomes more and more difficult until it becomes impossible. This data shows the breakdown of the edge modes under the influence of disorder. Clearly, there are limits to the topological protection, even though the feature of a vanishing energy of the edge modes persists as required.

The quantitative behavior of $|\langle \psi | \psi_{\text{cl}} \rangle|^2(k_x)$ as a function of σ is studied in Fig. 11(a). The transition probability decreases upon increasing σ . Beyond a certain value of σ the transition probability saturates at a small residual value. If the energy of the edge mode in the clean system is far away from the band edges of the continua (red curve, symbol 1) the transition probability decreases more slowly than if its energy is close to one of the continua (green curve, symbol 2).

In Fig. 11(b) we depict the dependence of the complete energy spectrum on the disorder strength. The modes assigned to the two momenta shown in Fig. 11(a) are highlighted by the two lines. There are regions where the eigenenergies are dense corresponding to the continua. The energies between the two dense regions at low and at high energies belong to the edge modes. The energies assigned to the two momenta evolve upon increasing σ . At some value of σ , which is specific for the momentum k_x of the mode, they enter the bulk continuum. The corresponding values of σ are indicated approximately by vertical dashed lines in both panels of Fig. 11. Beyond these disorder strengths it can no longer be decided whether the modes are true edge modes or whether they belong to the continuum states.

Yet even beyond the dashed lines the transition

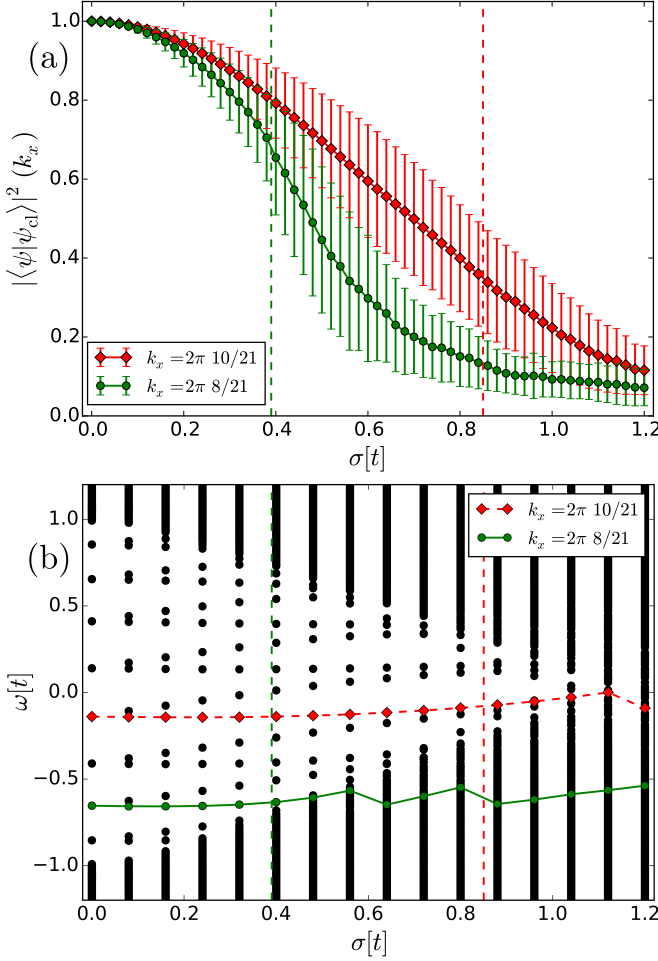


FIG. 11: (a) Transition probability $|\langle\psi|\psi_{cl}\rangle|^2(k_x)$ at two values of k_x for the right-moving edge state as a function of the disorder strength σ in a system with $N_y = 50$ and $N_x = 21$. The probability is averaged over 50 configurations. The error bars represent the standard deviation. The dashed lines depict where the edge modes enter the continuum of the bulk states. (b) Complete energy spectrum for an exemplary configuration. The energies highlighted in color correspond to the two values of k_x displayed in (a).

probability is large enough to assign energies to the momenta k_x . But it happens that the assigned energies jump as can be seen for $k_x = 2\pi 8/21$ where kinks occur beyond the dashed line. This indicates that the assignment energy \leftrightarrow momentum based on the transition probability is no longer reliable.

Next, we address the dependence of the modes on the width N_y and the length N_x of the system. Larger N_y increases the width of the strip. Since the edge modes are localized at the boundaries increasing the width separates them more and more and makes them independent from each other. We focused on wide enough strips anyway so that the edge modes are essentially independent of N_y . This is supported clearly by Fig. 12. The width N_y of the strip plays no important role once it is large enough. Furthermore, Fig. 12 shows that $|\langle\psi|\psi_{cl}\rangle|^2$ cru-

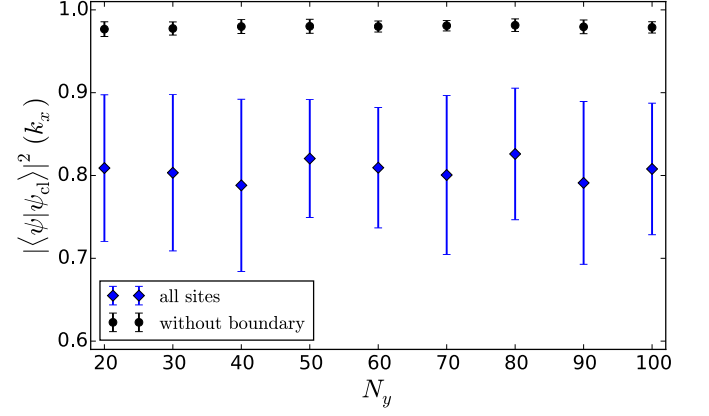


FIG. 12: (Color online) Transition probability $|\langle\psi|\psi_{cl}\rangle|^2$ at $k_x = 2\pi 8/21$ as a function of the width N_y of the strip of the Haldane model with $t_2 = 0.2t$, $\phi = \pi/2$, and a length of $N_x = 21$. The probability is averaged over 50 configurations for $\sigma = 0.1t$. The error bars represent a standard deviation. The effect of local disorder on all sites is shown by black circles. The blue (gray) circles depict the effect if disorder is only present in the bulk, but not at the edges. As to be expected, the edge modes are much less influenced in this case.

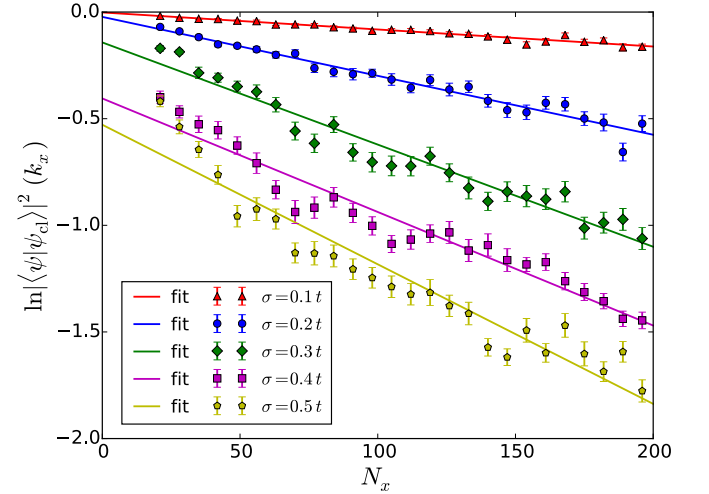


FIG. 13: (Color online) The logarithm of the transition probability at the momentum $k_x = 2\pi 10/21$ vs. the length N_x of the system at $t_2 = 0.2t$, $\phi = \pi/2$, and the width $N_y = 20$. The transition probability is averaged over 50 random configurations for various disorder strengths σ . The error bars represent the standard deviation of the average.

cially depends on the characteristics of the edges. If the edges are unaffected by the local disorder the transition probability takes significantly larger values than in the case where all sites are subject to random potentials.

Increasing the length N_x of the system has a pronounced effect on the transition probability as shown in Fig. 13. Note the logarithmic scale of the y-axis. Though the numerical data for the transition probability $|\langle\psi|\psi_{cl}\rangle|^2(k_x)$ is a bit noisy, it agrees well with an

σ	$a \pm \Delta a$	$\gamma \pm \Delta \gamma$
0.1	-0.00174 ± 0.00458	0.00080 ± 0.00004
0.2	-0.02261 ± 0.01491	0.00276 ± 0.00012
0.3	-0.14242 ± 0.02713	0.00479 ± 0.00023
0.4	-0.40515 ± 0.03240	0.00532 ± 0.00027
0.5	-0.52846 ± 0.04800	0.00654 ± 0.00040

TABLE I: Fitted values of the linear fits $\ln |\langle \psi | \psi_{cl} \rangle(N_x)|^2 \approx a - \gamma N_x$ in Fig. 13.

exponential dependence

$$|\langle \psi | \psi_{cl} \rangle|^2(k_x) \propto \exp(-\gamma(\sigma)N_x) \quad (10)$$

where the rate γ depends on the disorder strength. Naturally, the overlap decreases more rapidly if the disorder strength is larger.

The observed dependence on N_x can be understood as follows. Let us view a system of given length N_x to be formed by concatenating a number r of short subsystems of length n_x with $N_x = r \cdot n_x$. If the subsystems are still long enough, the physics inside of each of them is only negligibly influenced by the boundaries between them. Then, the transition probability of the total system is given by the product of all the transition probabilities of the subsystems

$$|\langle \psi | \psi_{cl} \rangle(N_x)|^2 = \prod_{j=1}^r |\langle \psi | \psi_{cl} \rangle(n_x, j)|^2. \quad (11)$$

On average, the transition probabilities of all the subsystems are the same so we denote them by $p_{sub} < 1$. Thus we have

$$|\langle \psi | \psi_{cl} \rangle(N_x)|^2 = p_{sub}^r \quad (12a)$$

$$= \exp(-\tilde{\gamma}r) \quad (12b)$$

$$= \exp(-\gamma N_x) \quad (12c)$$

where we set $p_{sub} = \exp(-\tilde{\gamma})$ and $\gamma = \tilde{\gamma}/n_x$.

Inspecting Fig. 13 reveals that the exponential decay does not apply for short systems, but only beyond a certain minimum length. Thus, the above argument is only approximately true because the assumption of negligible influence of the boundaries is not perfectly justified for short systems. Thus a linear fit $a - \gamma N_x$ of the logarithm of $|\langle \psi | \psi_{cl} \rangle(N_x)|^2$ as shown in Fig. 13 works well, but the offset a is not zero in contrast to what our simple argument suggests in Eq. (12c). The fitted values are given in Table I.

Finally, we study the effect of disorder on the edge mode at a decorated edge. It has been advocated that the decoration and a tunable gate voltage shifting the potential at the edges render the realization of tunable, direction-dependent delay lines possible³⁷. If we recall the extension to the Kane-Mele model a dependence on the spin is also possible. This makes the fundamental idea interesting for spintronics as well. But for all applications the robustness towards imperfections is decisive. This motivates the investigation of disorder.

The purpose of the decoration is to reduce the Fermi velocity by design, i.e., to introduce fairly flat regions in the dispersion. This implies that there are many eigenstates of very similar energies. From perturbation theory one knows that such systems are susceptible to generic perturbations such as disorder. We investigate a system of size $N_y = 50$ and $N_x = 21$ with a decorated upper boundary. Since the decorating sites are not excluded from disorder we also add a random local potential to the additional sites. In the reconstruction of the dispersion of the edge modes we require a certain minimum transition probability in order to obtain a reliable mapping between momenta and eigenstates. From the above results for systems of the considered size we set this threshold to 0.3, cf. Figs. 10 and 11. For weak disorder the successfully reconstructed dispersion is displayed in Fig. 14(a).

For stronger disorder, a complete reconstruction of the dispersion of the edge states turns out to be impossible, see Fig. 14(b). For instance for $\sigma = 0.1t$, the eigenstates with energies within the flat dispersion in the center of the gap cannot be mapped reliably to the corresponding momenta because their overlap falls below the threshold. As expected from our perturbative argument, the states in the flatter regions of the dispersion are not particularly robust against disorder.

For a complete understanding, we also studied the case where there is no disorder at the decorating sites. This is a realistic scenario if the technique which creates the decorating sites is a different one from the one growing the bulk. Clearly, this kind of disorder has much less detrimental effects on the edge modes, see for instance Fig. 12. The edge modes are rather localized at the decorating sites so that they are less exposed to disorder. This holds in particular for the states with rather flat dispersion because they differ only slightly from the completely local states on the decorating sites. For instance the same configuration as used in Fig. 14(b) can be reconstructed up to much stronger disorder $\sigma = 0.5t$ if the disorder is restricted to the bulk.

Note that the above observations do not contradict to the general idea of topological protection because there are modes at arbitrary small energies. But for transmitting signals one needs a clearly defined dispersion $\omega(k_x)$ which yields the group velocity $\partial\omega/\partial k_x$. If this is not the case as we found here for stronger disorder we presume that the system is not suitable for applications based on signal transmission. This sets certain limits to the general idea of topological protection which should not be misunderstood as a guarantee that dispersion and group velocity are well-defined.

V. SUMMARY

In this paper, we concentrated on the Fermi velocity of the edge states of topologically nontrivial fermionic lattice systems. The Fermi velocity is the group velocity with which signals can be transmitted through the edge

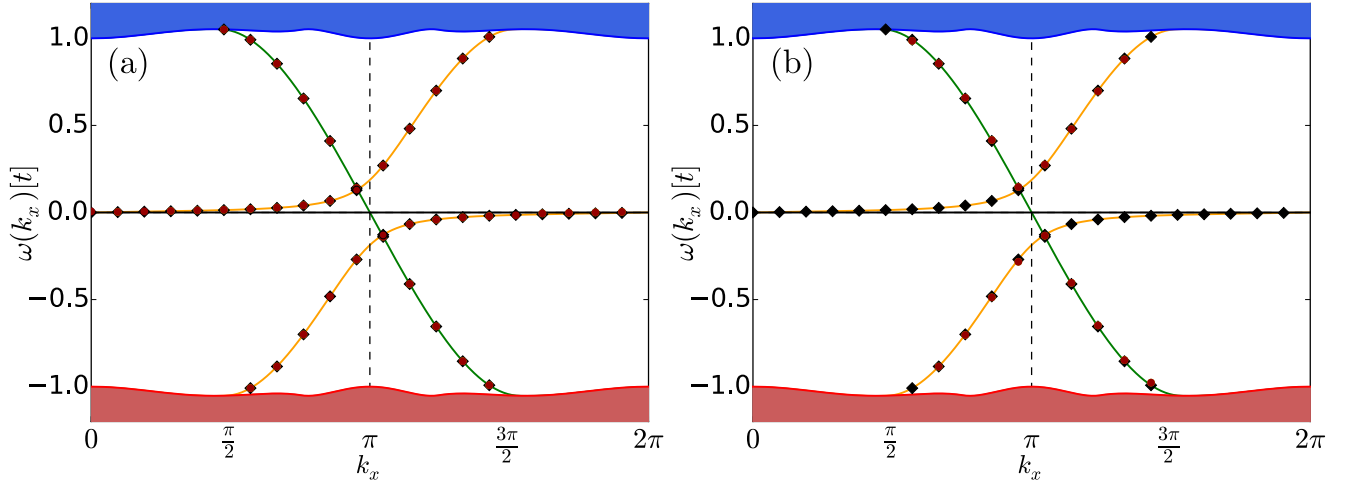


FIG. 14: (Color online) Dispersion of the edge states in a decorated system with $t_2 = 0.2t$, $\lambda_t = 0.2t$, and $\phi = \pi/2$. The filled areas indicate the continua of bulk states. The right-moving edge state marked in orange (light gray) is located at the top edge while the left-moving edge state marked in green (dark gray) is located at the bottom edge. For reference, the black diamonds depict the reconstructed dispersion in the clean system with $N_y = 50$ and $N_x = 21$ while the red (gray) circles depict the reconstructed dispersion for $\sigma = 0.001t$ in panel (a) and for $\sigma = 0.1t$ in panel (b). Note that in panel (b) the flat part of the dispersion could not be reconstructed because the transition probabilities fall below the required threshold, see main text.

states. The tunability of the edge states can be used to create delay lines based on interference, see Ref. 37. Thus it is a measurable quantity very important for transport behavior, but which is different from DC conductivity studied previously^{35,36}.

First, in Sec. II, we presented the decorated Haldane model to be able to compare later to the extended Kane-Mele model and to the decorated Haldane model with disorder. We discussed the effects that various parameters of the decoration have on the properties of the edge states, most notably on their dispersion. The Fermi velocity is direction-dependent if the different edges are decorated and tuned independently.

Second, in Sec. III, the results for the spinless Haldane model were extended to the spinful Kane-Mele model. In this model, the dispersions of the edge modes depend on the combination of direction and spin. The model in its entire composition does not break TRS. So for each right (or left)-moving spin \uparrow mode there is a left (or right)-moving spin \downarrow mode with equal energy. The full control of the dispersions and their dependence on direction and spin *separately* can be achieved by realizing spin-dependent exchange couplings at the edges. Candidates for the realization of such terms in the Hamiltonian are the proximity effect of a ferromagnet in hybrid structures or magnetic doping in the bulk of the system. In addition, we studied the effect of Rashba coupling.

Third, in Sec. IV, we addressed the effect of disorder on the edge states as motivated by the fundamental paradigm of topological effects that the edge states are particularly robust against any kind of perturbation. For clarity, we performed this study for the spinless Haldane model. Indeed, the existence of gapless states at the edges is guaranteed by topological protection. But there

is no guarantee for the preservation of a well-defined dispersion of the edge modes. Thus, the transport properties are likely to be influenced significantly by disorder.

We reconstructed the dispersion of the edge modes in disordered systems by comparing them with the edge modes of the clean system. The transition probability between the edge state in the clean system and the one in the disordered system served as criterion to identify the modes. In this way, one can link the eigenstates in the disordered systems to certain momenta and re-define a dispersion. The approach works very well for edge states of which the energy is far away from the continua. But if the energies approach the band edges, the mapping becomes ambiguous so that its application is no longer reliable. Thus, for stronger disorder only small parts of the original dispersions can be reconstructed. Increasing the disorder even further eventually destroys the edge modes completely. In addition, we established an approximate formula for the reduction of the bulk gap due to disorder in the Haldane model.

Furthermore, we clarified how the transition probability depends on the width and the length of the system under study. The width does not have a significant impact once the sample is wide enough so that the two edge modes do not interact anymore. The increasing of the length leads to an exponential decrease of the transition probability.

Finally, we addressed the robustness of the edge states at decorated edges which allow us to design small and tunable Fermi velocities. Applying the reconstruction procedure we could cope with small disorder strengths. But we found our expectation confirmed that the flat regions of the dispersions are particularly susceptible to perturbations. We conclude that in order to realize and

to apply the ideas of tunable group velocities one has to resort to clean samples or, at least, to samples where the decorating sites are not subject to disorder. The edge modes displaying a large dispersion and staying away from the band edges of the bulk modes are those which are most robust to disorder.

Further studies are necessary in order to investigate the influence of other kinds of disorder or imperfections. On the one hand, it is conceivable that spatially correlated disorder is less harmful to the edge modes than the completely local one we studied here. The edge modes may flow around smoother regions of disorder or imperfections, for an example on the surface of a topological insulator, see Ref. 47. On the other hand, imperfections

such as vacancies can behave like a local infinite potential, i.e., having very drastic effects on the edge modes.

Extending such investigations to other kinds of systems displaying topological order constitutes another broad field of research.

Acknowledgments

This work was supported by the Deutsche Forschungsgemeinschaft and the Russian Foundation of Basic Research in the International Collaborative Research Center TRR 160.

-
- * Electronic address: maik.malki@tu-dortmund.de
- ¹ K. v. Klitzing, G. Dorda, and M. Pepper, Phys. Rev. Lett. **45**, 494 (1980).
 - ² D. C. Tsui, H. L. Stormer, and A. C. Gossard, Phys. Rev. Lett. **48**, 1559 (1982).
 - ³ Y. Hatsugai, Phys. Rev. Lett. **71**, 3697 (1993).
 - ⁴ D. J. Thouless, M. Kohmoto, M. P. Nightingale, and M. den Nijs, Phys. Rev. Lett. **49**, 405 (1982).
 - ⁵ J. E. Avron, R. Seiler, and B. Simon, Phys. Rev. Lett. **51**, 51 (1983).
 - ⁶ Q. Niu, D. J. Thouless, and Y.-S. Wu, Phys. Rev. B **31**, 3372 (1985).
 - ⁷ M. Kohmoto, Ann. of Phys. **160**, 343 (1985).
 - ⁸ G. S. Uhrig, Z. Phys. B **82**, 29 (1991).
 - ⁹ M. V. Berry, Phys. Roy. Soc. Lond. **A 392**, 45 (1984).
 - ¹⁰ F. D. M. Haldane, Phys. Rev. Lett. **61**, 2015 (1988).
 - ¹¹ C. H. Redder and G. S. Uhrig, Phys. Rev. A **93**, 033654 (2016).
 - ¹² H. Weng, R. Yu, X. Hu, X. Dai, and Z. Fang, Adv. Phys. **64**, 227 (2015).
 - ¹³ C.-X. Liu, S.-C. Zhang, and X.-L. Qi, Annu. Rev. Condens. Matter Phys. **7**, 301 (2016).
 - ¹⁴ Y. Ren, Z. Qiao, and Q. Niu, Rep. Prog. Phys. **79**, 066501 (2016).
 - ¹⁵ C. L. Kane and E. J. Mele, Phys. Rev. Lett. **95**, 146802 (2005).
 - ¹⁶ C. L. Kane and E. J. Mele, Phys. Rev. Lett. **95**, 226801 (2005).
 - ¹⁷ M. Z. Hasan and C. L. Kane, Rev. Mod. Phys. **82**, 3045 (2010).
 - ¹⁸ L. Fu and C. L. Kane, Phys. Rev. B **74**, 195312 (2006).
 - ¹⁹ A. B. Bernevig and T. L. Hughes, *Topological Insulators and Topological Superconductors* (Princeton University Press, Princeton, 2013).
 - ²⁰ C. Wu, B. A. Bernevig, and S.-C. Zhang, Phys. Rev. Lett. **96**, 106401 (2006).
 - ²¹ X.-L. Qi and S.-C. Zhang, Rev. Mod. Phys. **83**, 1058 (2011).
 - ²² B. A. Bernevig, T. L. Hughes, and S.-C. Zhang, Science **314**, 1757 (2006).
 - ²³ M. König, S. Wiedmann, C. Brüne, A. Roth, H. Buhmann, L. W. Molenkamp, X.-L. Qi, and S.-C. Zhang, Science **318**, 766 (2007).
 - ²⁴ A. Roth, C. Brüne, H. Buhmann, L. W. Molenkamp, J. Maciejko, X.-L. Qi, and S.-C. Zhang, Science **325**, 294 (2009).
 - ²⁵ I. Knez, R.-R. Du, and G. Sullivan, Phys. Rev. Lett. **107**, 136603 (2011).
 - ²⁶ L. Du, I. Knez, G. Sullivan, and R.-R. Du, Phys. Rev. Lett. **114**, 096802 (2015).
 - ²⁷ C.-C. Liu, W. Feng, and Y. Yao, Phys. Rev. Lett. **107**, 076802 (2011).
 - ²⁸ C.-Z. Chang, J. Zhang, X. Feng, J. Shen, Z. Zhang, M. Guo, K. Li, Y. Ou, P. Wei, L.-L. Wang, Z.-Q. Ji, Y. Feng, S. Ji, X. Chen, J. Jia, X. Dai, Z. Fang, S.-C. Zhang, K. He, Y. Wang, L. Lu, X.-C. Ma, and Q.-K. Xue, Science **340**, 167 (2013).
 - ²⁹ X. Kou, S.-T. Guo, Y. Fan, L. Pan, M. Lang, Y. Jiang, Q. Shao, T. Nie, K. Murata, J. Tang, Y. Wang, L. He, T.-K. Lee, W.-L. Lee, and K. L. Wang, Phys. Rev. Lett. **113**, 137201 (2014).
 - ³⁰ C.-Z. Chang, W. Zhao, D. Y. Kim, H. Zhang, B. A. Assaf, D. Heiman, S.-C. Zhang, C. Liu, M. H. W. Chan, and J. S. Moodera, Nature Mat. **14**, 473 (2015).
 - ³¹ S.-C. Wu, G. Shan, and B. Yan, Phys. Rev. Lett. **113**, 256401 (2014).
 - ³² Y. Han, J.-G. Wan, G.-X. Ge, F.-Q. Song, and G.-H. Wang, Sci. Rep. **5**, 16843 (2015).
 - ³³ A. V. Krasheninnikov and R. M. Nieminen, Theor. Chem. Acc **129**, 625 (2011).
 - ³⁴ G. Jotzu, M. Messer, R. Desbuquois, M. Lebrat, T. Uehlinger, D. Greif, and T. Esslinger, Nature **515**, 237 (2014).
 - ³⁵ J. S. Van Dyke and D. K. Morr, Phys. Rev. B **93**, 081401(R) (2016).
 - ³⁶ Z. Qiao, Y. Han, L. Zhang, K. Wang, X. Deng, H. Jiang, S. A. Yang, J. Wang, and Q. Niu, Phys. Rev. Lett. **117**, 056802 (2016).
 - ³⁷ G. S. Uhrig, Phys. Rev. B **93**, 205438 (2016).
 - ³⁸ Y. A. Bychkov and E. I. Rashba, J. Phys. C **17**, 6039 (1984).
 - ³⁹ S. A. Wolf, D. D. Awschalom, R. A. Buhrman, J. M. Daughton, S. von Molnár, M. L. Roukes, A. Y. Chtchelkanova, and D. M. Treger, Science **294**, 1488 (2001).
 - ⁴⁰ I. Žutić, J. Fabian, and S. Das Sarma, Rev. Mod. Phys. **76**, 323 (2004).
 - ⁴¹ H. A. Kramers, Proc. Koninklijke Akademie van Wetenschappen **33**, 959 (1930).

- ⁴² Z. Jiang, C.-Z. Chang, C. Tang, J.-G. Zheng, J. S. Moodera, and J. Shi, AIP Advances **6**, 055809 (2016).
- ⁴³ T. Jungwirth, J. Sinova, J. Mašek, J. Kučera, and A. H. MacDonald, Rev. Mod. Phys. **78**, 809 (2006).
- ⁴⁴ Z. Qiao, S. A. Yang, W. Feng, W.-K. Tse, J. Ding, Y. Yao, J. Wang, and Q. Niu, Phys. Rev. B **82**, 161414(R) (2010).
- ⁴⁵ T.-W. Chen, Z.-R. Xiao, D.-W. Chiou, and G.-Y. Guo, Phys. Rev. B **84**, 165453 (2011).
- ⁴⁶ M. Fruchart and D. Carpentier, Comptes Rendus Physique **14**, 779 (2013).
- ⁴⁷ S. Bauer and C. A. Bobisch, Nature Comm. **7**, 11381 (2016).